Study of the energy level scheme of Pr^{3+}:LaOCl under pressure

1998 J. Phys.: Condens. Matter 10 9329

(http://iopscience.iop.org/0953-8984/10/41/015)

J. Phys.: Condens. Matter **10** (1998) 9329–9342. Printed in the UK PII: S0953-8984(98)95486-8

Study of the energy level scheme of Pr^{3+}:LaOCl under pressure

C Bungenstock†, Th Tröster†, W B Holzapfel†, R Bini‡, L Ulivi§ and S Cavalieri‖

† FB 6 Physik, Universität-GH-Paderborn, 33095 Paderborn, Germany

‡ Dipartimento di Chimica, Università di Firenze, Via G Capponi 9, 50121 Firenze, Italy, and European Laboratory for Non-Linear Spectroscopy (LENS), Largo E Fermi 2, 50124 Firenze, Italy

§ Instituto di Elettronica Quantistica (CNR), Via Panciatichi 56/30, 50127 Firenze, Italy

‖ Dipartimento di Fisica, LENS and INFM, Università di Firenze, Largo E Fermi 2, 50125 Firenze, Italy

Received 30 June 1998

Abstract. Excitation and luminescence spectra of Pr^{3+} in LaOCl were measured over the spectral range from 11 000 cm^{-1} to 22 000 cm^{-1}. At ambient pressure a total of 46 spectral lines could be observed. Under pressures up to 16 GPa, all lines exhibit a red-shift—however, with very different rates. From the spectral lines, the energy level scheme of the $4f^2$ configuration could be partly derived. From 37 levels at ambient pressure, 30 could also be obtained under pressure. The energy level scheme is described by the use of free-ion (F^k ($k = 2, 4, 6$), α, β, γ, ζ) and crystal-field parameters (B_0^2, B_0^4, B_4^4, B_0^6, B_6^6). According to the so-called nephel-auxetic effect, the free-ion parameters F^k and ζ decrease under pressure. The magnitudes of the variations depend on the selected energy levels. Surprisingly the crystal-field strength shows a peculiar behaviour with an initial decrease and a minimum at 15 GPa. This behaviour can be explained within the context of the superposition model.

1. Introduction

The energy levels of lanthanide ions in different compounds have been the subject of many studies in the last few decades [1–3]. However, high-pressure studies have been performed only in a limited number of cases, where they were very useful for the assignment of lines and for more detailed studies of the crystal-field splittings [4–7]. The main advantage of the application of high pressure is the possibility of continuously tuning the interatomic distances and therefore the crystal-field strength in a given sample. At the same time and in contrast to the case for other comparative studies of different samples, neither the point symmetry of the lanthanide sites nor the chemical environment is changed.

In detail, the influence of pressure on crystal fields was studied for Ln^{3+} in $LaCl_3$ (Ln = Pr, Nd) [4, 8] and U^{3+} in $LaCl_3$ [5], where a phase transition occurs at around 8 GPa, limiting the available pressure range in the former studies [4]. To extend the pressure range and therefore the variation in crystal-field strength, LaOCl was chosen as a host material for the present work.

The host LaOCl was doped with the Pr^{3+} ion. An advantage of Pr^{3+} is its relatively small number of energy levels which allows one to obtain almost complete information on the energy level scheme. The relatively small matrices need less time for computing and,

0953-8984/98/419329+14$19.50

in addition, the parametrization is easier for only two f electrons, because three-particle interactions can be neglected.

Former studies on Pr^{3+}:LaOCl and PrOCl yielded up to 50 energy levels [9, 10]. From these levels, Coulomb interaction, spin–orbit coupling, and crystal-field parameters have been determined. However, the energy levels given in these two investigations show large discrepancies. Therefore, one task of the present work was to check the assignment of the various lines, where high pressure can give additional information.

2. Experimental procedure

Absorption and luminescence spectroscopy are widely used to obtain information about energy levels of lanthanide ions in transparent host crystals. If both methods are combined, one usually obtains a much larger part of the energy level scheme. However, absorption spectroscopy often cannot be applied, when the dopants are very dilute, especially in the case of high-pressure experiments, where the samples are very thin (10 μm to 40 μm).

For the complete characterization of the electronic energy levels, luminescence spectroscopy alone is often not sufficient, because nonradiative relaxations between different excited states can quench the luminescence of the excited states. To avoid these problems, excitation spectroscopy can be used, resulting in additional information being obtained about excited states.

The present experiments were performed with two different experimental set-ups. In the first set-up (at the University of Paderborn) an argon-ion laser is used either to directly excite the luminescence of the sample or to pump a dye laser system. Due to the limitations of the given pump laser, only Rhodamin 6G could be pumped efficiently, which limits the range for excitation spectroscopy to 14 000 cm^{-1} to 17 000 cm^{-1}.

Pressures were generated with a small diamond anvil cell (with a pressure range up to 25 GPa) and measured by the ruby luminescence method using the linear ruby scale [11] with constant thermal corrections [12]. A closed-cycle refrigerator provided temperatures of about 20 K. The pressure-transmitting medium was nitrogen.

In the second set-up (at the University of Florence), the third harmonic of a pulsed Nd-YAG laser pumped a dye laser at a rate of 10 Hz. Various dyes were used for different wavelength regions which cover a range from 20 400 cm^{-1} to 22 500 cm^{-1}. Typical pulse energies ranged from 40 to 100 μJ.

After an excitation pulse of 6 ns duration from the laser system, the detector gate opened typically with a delay of 0.8 ms for about 10 ms duration. During this time the signals from the photomultiplier were acquired in photon-counting mode. This procedure reduced first of all spurious signals from reflected laser light and optimized the detected signal-to-noise ratio when the gate length was adjusted to about two to three times the decay time of the acquired luminescence signal.

In this case, a membrane diamond anvil cell similar to that described in reference [13] mounted on the cold finger of a closed-cycle refrigerator generates the high pressure, with argon as the pressure-transmitting medium. The pressures were determined from the shift of one strong excitation line ($^3H_4(E) \rightarrow {}^3P_0(A1)$), for which the pressure dependence had been determined already in luminescence measurements.

The LaOCl samples with 1 mol% Pr^{3+} were synthesized in the crystal growth laboratory of the University of Paderborn.

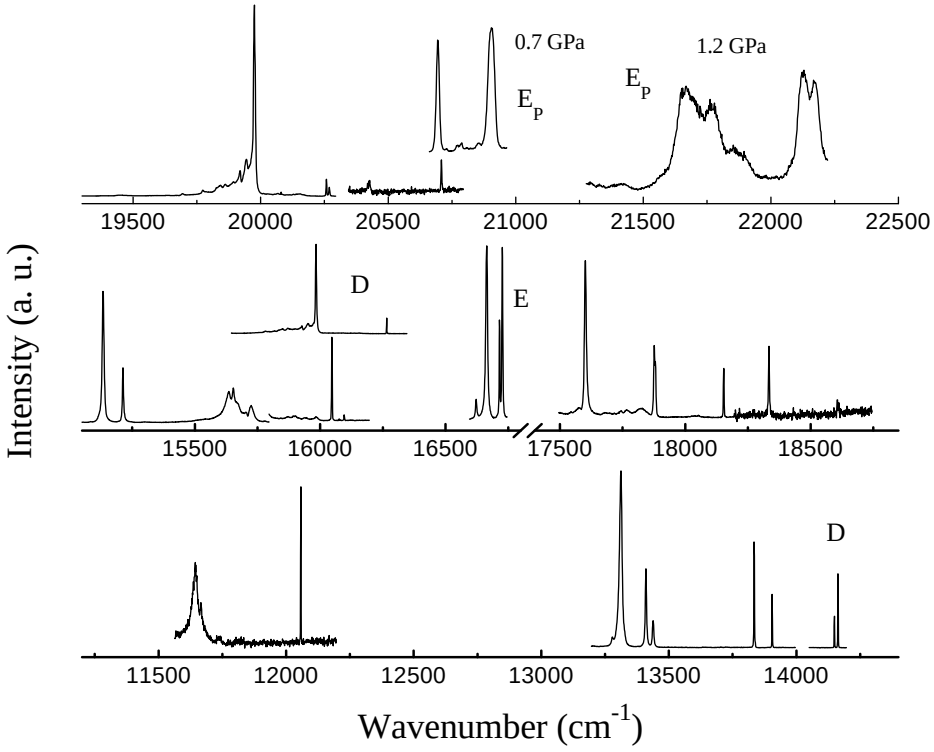

Figure 1. Luminescence and excitation spectra (E) of Pr^{3+}:LaOCl at ambient pressure at low temperatures (20 K/60 K). The luminescence spectra were excited with an argon-ion laser; the spectrum marked D was resonantly excited with a dye laser system. The excitation spectra above 20 700 cm^{-1} were taken at 0.7 GPa and 1.2 GPa, respectively.

3. Ambient-pressure results

At ambient pressure it was possible to observe luminescence transitions from $^3P_1$, $^3P_0$, and $^1D_2$ to ^3H_J ($J = 4, 5, 6$) and ^3F_J ($J = 2, 3, 4$). In addition, excitation spectroscopy yielded further information about $^1D_2$, $^1I_6$, and $^3P_2$. Figure 1 gives an overview of all of the luminescence and excitation spectra (marked E and E_P) observed in the range from 11 500 cm^{-1} to 22 500 cm^{-1}. Note that the excitation spectra above 20 700 cm^{-1} (E_P) were not taken at ambient pressure, but at 0.7 GPa and 1.2 GPa, respectively. Although no ambient-pressure spectra were collected, it was possible to extrapolate the line positions to their ambient-pressure values with the help of their pressure dependences.

The luminescence spectra shown in figure 1 were excited with the argon-ion laser. The only exceptions are the spectra marked D, where the dye laser system was used to resonantly excite the Pr^{3+} ion. In general, transitions originating from $^3P_0$ dominate over all of the other lines. Also weakly observable were transitions from $^3P_1$ and $^1D_2$, while $^3P_2$ did not show any luminescence.

Due to the broad structure of the excitation spectra above 21 500 cm^{-1}, the analysis and assignment of these lines was complicated. Nevertheless, the various lines became much clearer under pressure, where it was possible to distinguish four electronic transitions.

Table 1 gives all of the lines which could be unambiguously assigned. The only doubtful case in this table is the line at 19 692.5 cm^{-1}, which can also be attributed to a vibronic

Table 1. Luminescence and excitation lines of Pr^{3+}:LaOCl at ambient pressure and low temperatures (20 K/60 K). Extrapolated lines from high-pressure spectra are given with an estimated error in parentheses.

Transition			Energy (cm^{-1})	Transition			Energy (cm^{-1})
$^3H_4(E)$	→	$^3P_2(A_1)$	22 212 (3)	$^3H_4(E)$	→	$^1D_2(B_1)$	16 664.0
		$^3P_2(E)$	22 164 (3)	$^3H_4(B_1)$	→	$^1D_2(B_1)$	16 622.2
		$^3P_2(B_1)$	21 925 (5)	$^1D_2(B_2)$	→	$^3H_4(E)$	16 265.3
		$^3P_2(B_2)$	21 838 (10)	$^3P_0(A_1)$	→	$^3H_6(A_1)$	16 095.8
$^3H_4(A_1)$	→	$^3P_1(E)$	20 912 (3)			$^3H_6(E)$	16 046.7
$^3H_4(E)$	→	$^3P_1(E)$	20 912 (3)	$^1D_2(B_2)$	→	$^3H_4(E')$	15 983.2
		$^1I_6(B_2)$	20 794 (3)	$^3P_0(A_1)$	→	$^3H_6(E')$	15 725.6
		$^1I_6(E)$	20 777 (3)			$^3H_6(A_1')$	15 653.6
		$^3P_1(A_2)$	20 707 (3)			$^3H_6(E'')$	15 634.9
$^3P_1(A_2)$	→	$^3H_4(E)$	20 707.4	$^3P_0(A_1)$	→	$^3F_2(E)$	15 213.3
		$^3H_4(E')$	20 424.9			$^3F_2(A_1)$	15 134.0
$^3P_0(A_1)$	→	$^3H_4(A_1)$	20 267.8	$^1D_2(B_2)$	→	$^3H_5(E)$	14 163.1
		$^3H_4(E)$	20 256.5			$^3H_5(B_2)$	14 148.9
		$^3H_4(E')$	19 974.3	$^3P_0(A_1)$	→	$^3F_3(E)$	13 905.1
		$^3H_4(A_1')$	19 692.5	$^1D_2(B_2)$	→	$^3H_5(E')$	13 890.8
$^3P_1(A_2)$	→	$^3H_5(A_2)$	18 611.3	$^3P_0(A_1)$	→	$^3F_3(E')$	13 834.5
		$^3H_5(E)$	18 604.3	$^1D_2(B_2)$	→	$^3H_5(E'')$	13 611.1
		$^3H_5(E')$	18 332.3	$^3P_0(A_1)$	→	$^3F_4(E)$	13 438.6
$^3P_0(A_1)$	→	$^3H_5(E)$	18 153.5			$^3F_4(A_1)$	13 410.2
		$^3H_5(E')$	17 880.8			$^3F_4(E')$	13 312.2
		$^3H_5(A_1)$	17 875.8			$^3F_4(A_1')$	13 278.4
		$^3H_5(E'')$	17 601.8	$^1D_2(B_2)$	→	$^3H_6(E)$	12 057.5
$^3H_4(A_1)$	→	$^1D_2(A_1)$	16 726.6			$^3H_6(E')$	11 735.3
$^3H_4(E)$	→	$^1D_2(A_1)$	16 715.5			$^3H_6(E'')$	11 644.3

side band of the $^3P_0(A_1) \rightarrow {}^3H_4(E')$ transition. Due to this uncertainty, $^3H_4(A_1')$ was not taken into account for the parameter analysis. In any case, it made no significant difference to the parameter values whether $^3H_4(A_1')$ was added or not. From the observed spectral lines, 37 energy levels were obtained as given in table 2.

There are some discrepancies between the positions of the levels as obtained in this work and those obtained from former investigations. Parts of these discrepancies may be explained by a concentration effect, which means that an enhanced Pr^{3+} concentration in LaOCl will lead to shorter bond lengths and therefore to an increased internal pressure on the Pr^{3+} ion. The limit is reached in the case of the pure substance PrOCl, where the lattice constants are more than 1% smaller than for LaOCl.

From some preliminary studies on PrOCl as well as from the high-pressure shifts of the energy levels, it is easy to estimate that the concentration effect can result in shifts of not more than 50 cm^{-1} for higher-lying levels such as ^3P_J ($J = 0, 1, 2$). Taking into account this result, it becomes possible to explain some of the discrepancies between the different studies. As an example consider the single level $^3P_0(A_1)$. The energies found for $^3P_0(A_1)$ are: 20 267.8 cm^{-1} (I: present work, 1% Pr^{3+}:LaOCl), 20 259 cm^{-1} (II: Mazurak *et al* [9], Pr^{3+}:LaOCl; concentration not explicitly given, but between 1% and 30%), and 20 242 cm^{-1} (III: Antic-Fidancev *et al* [10], PrOCl). The different values can be explained

Table 2. Experimental and calculated energy levels of Pr^{3+}:LaOCl at ambient pressure. Extrapolated energies from high-pressure spectra are given with an estimated error in parentheses.

		Energy (cm^{-1})				Energy (cm^{-1})	
Level		Experimental	Calculated	Level		Experimental	Calculated
$^3H_4$	A_1	0.0	−5.0	$^3F_4$	A_1	6857.6	6836.0
	E	11.2	17.3		A_2	—	6867.1
	B_1	—	73.3		B_2	—	6955.2
	E′	293.5	291.2		E′	6955.6	6987.7
	B_2	321.3	330.6		A_1'	6989.4	7014.3
	A_2	—	521.6				
	A_1'	575.3	559.9	$^1G_4$	B_1	—	9582.3
					E	—	9758.3
$^3H_5$	A_2	2107.3	2111.4		A_1	—	9880.0
	E	2114.0	2125.5		A_2	—	9936.6
	B_2	2127.6	2145.7		B_2	—	9955.0
	B_1	—	2372.8		E′	—	10 063.4
	E′	2386.4	2369.9		A_1'	—	10 081.9
	A_1	2392.0	2379.6				
	A_2'	2449.7	2450.3	$^1D_2$	B_2	16 277.5	16 258.3
	E″	2665.7	2644.5		B_1	16 675.1	16 673.1
					A_1	16 726.6	16 758.7
$^3H_6$	A_1	4172.0	4187.9		E	—	16 793.9
	E	4220.1	4237.4				
	B_1	—	4303.3	$^3P_0$	A_1	20 267.8	20 263.2
	A_2	—	4516.8				
	E′	4542.2	4532.8	$^3P_1$	A_2	20 718.6	20 723.2
	B_2	—	4539.9		E	20 924 (3)	20 932.1
	A_1'	4614.2	4605.0				
	E″	4632.6	4626.1	$^1I_6$	A_1	—	20 782.4
	B_1'	—	4893.4		E	20 789 (3)	20 783.5
	B_2'	—	4914.1		B_2	20 805 (3)	20 794.8
					B_1	—	21 183.2
$^3F_2$	B_1	—	4946.9		E′	—	21 250.7
	B_2	—	4983.3		A_2	—	21 395.9
	E	5054.5	5061.2		A_1'	—	21 493.2
	A_1	5133.8	5138.0		E″	—	21 674.6
					B_2'	—	21 734.0
$^3F_3$	E	6362.7	6337.6		B_1'	—	21 746.8
	B_1	—	6402.8				
	E′	6433.3	6445.7	$^3P_2$	B_2	21 849 (10)	21 856.1
	B_2	—	6414.7		B_1	21 937 (5)	21 919.8
	A_2	—	6520.1		E	22 175 (3)	22 177.5
					A_1	22 224 (3)	22 224.0
$^3F_4$	B_1	—	6784.0				
	E	6829.2	6813.8	$^1S_0$	A_1	—	46 220.4

by the increasing pressure on the Pr^{3+} ion, when going from the small concentration to the pure substance. On this basis, the concentration in II was probably around 10%.

An example which cannot be explained by concentration effects is the $^1D_2(B_2)$ level. The energies found are: 16 277.5 cm^{-1} (I), 16 220^{-1} (II), and 16 295 cm^{-1} (III). The value in II should lie between the other two values, which is not the case. Antic-Fidancev *et al* argued that trap sites and impurities may have had a pronounced effect on the luminescence spectra in II, which could result in misinterpretation of the spectra.

The energy level scheme determined from luminescence and excitation spectra can now be used to extract various parameters, belonging to the free-ion and crystal-field part of the total Hamiltonian of the system. The free-ion part consists of the Coulomb interaction (Slater parameters F^2, F^4, F^6), spin–orbit coupling (ζ), configuration interaction (α, β, γ), and minor corrections for spin–spin and spin–other-orbit interactions (M^0, M^2, M^4) and the electrostatically correlated spin–orbit interaction (P^2, P^4, P^6). The second part, the crystal field, is treated as a perturbation of the free-ion part, and introduces the crystal-field parameters (B_0^2, B_0^4, B_4^4, B_0^6, B_4^6).

Table 3. Free-ion and crystal-field parameters (in cm^{-1}) for Pr^{3+}:LaOCl and PrOCl [10] at ambient pressure. Parameter errors are given in the brackets, where an asterisk marks a parameter which was kept fixed in the fits.

	Pr^{3+}:LaOCl		Pr^{3+}:PrOCl	
E_{ave}	9968	(8)	9955	—
F^2	67 307	(36)	67 659	—
F^4	50 097	(188)	49 458	—
F^6	32 989	(98)	32 814	—
ζ	742.2	(1.7)	742	(1)
α	22	(∗)	23.6	(1)
β	−700	(∗)	−676	(2)
γ	1422	(∗)	1422	(∗)
M_0	1.76	(∗)	—	—
P^2	275	(∗)	—	—
B_0^2	−855	(22)	−842	(9)
B_0^4	−440	(74)	−550	(24)
B_4^4	± 949	(32)	± 826	(16)
B_0^6	653	(97)	1092	(37)
B_4^6	± 160	(87)	± 27	(27)
N	37		50	
σ	16.9		17	

The results for these parameters are given in table 3. Also shown are the parameter values from the former study on PrOCl [10], which do not differ significantly from the present data, taking into account the concentration effect. The standard deviation obtained in the fits of the energy levels is 17 cm^{-1} in both studies.

4. High-pressure results

When high pressure is applied, all lines shift to lower wavenumbers—however, with different rates. Responsible for the overall red-shift (the nephelauxetic effect) is the weakening of the Coulomb and spin–orbit interaction between the f electrons. In general, the higher the energy of a given multiplet, the larger the observed red-shift. Superimposed on this red-shift are small variations in the crystal-field splittings, which in fact lead to the different pressure dependences observable for different transitions from the same multiplet.

From the 37 energy levels assigned at ambient pressure, only 30 could be observed up to 16 GPa. The main reason is the broadening of the lines, which results in an increased overlap, and the weakening of some transitions. On the other hand, a few special transitions were clearly observed only at higher pressures, like for example the transitions $^3H_4(E) \rightarrow {}^3P_2(B_1)$ and $^3H_4(E) \rightarrow {}^3P_2(B_2)$.

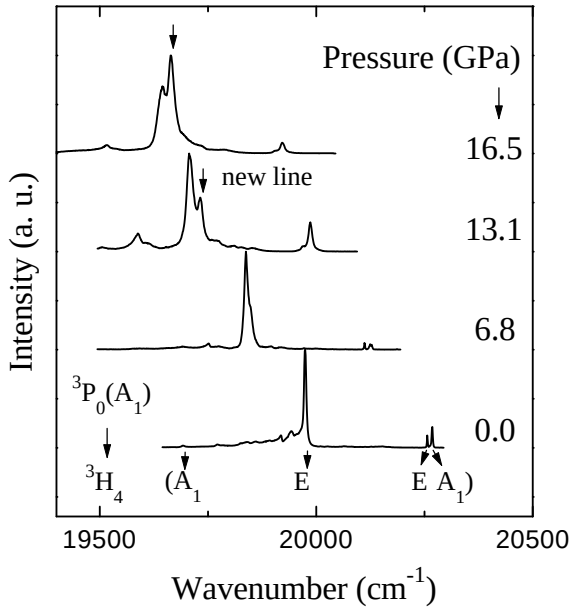

Figure 2. Luminescence spectra of Pr^{3+}:LaOCl at various pressures at 20 K.

Figure 2 shows some typical luminescence spectra of the transition $^3P_0 \rightarrow {}^3H_4$ at various pressures. Due to the selection rules in C_{4v} point symmetry, four luminescence lines are allowed, but only three could be assigned unambiguously at ambient pressure. The fourth line should lie approximately 300 cm^{-1} below the $^3P_0(A_1) \rightarrow {}^3H_4(E')$ transition and was only tentatively assigned at ambient pressure to a line at 19 692.5 cm^{-1}.

With increasing pressure, the red-shift of all lines is clearly visible. Besides this shift, two further observations can be made. First, a new line emerges on the high-energy side of the $^3P_0(A_1) \rightarrow {}^3H_4(E')$ transition, which cannot be assigned to another allowed transition, and, second, the relative intensity of the $^3P_0(A_1) \rightarrow {}^3H_4(A_1)$ line with respect to the $^3P_0(A_1) \rightarrow {}^3H_4(E)$ and $^3P_0(A_1) \rightarrow {}^3H_4(E')$ lines shows drastic changes from one spectrum to the other.

The changes in relative intensities can be caused by different sample orientations together with polarization effects. In fact, the spectra in figure 2 correspond to different samples

in different preparations. In addition, the $^3P_0(A_1) \rightarrow {}^3H_4(A_1)$ transition is π-polarized, whereas the other two transitions are σ-polarized. This means that the intensity of the transition $^3P_0(A_1) \rightarrow {}^3H_4(A_1)$ relative to those of the transitions $^3P_0(A_1) \rightarrow {}^3H_4(E)$ and $^3P_0(A_1) \rightarrow {}^3H_4(E')$ changes, if the orientation of the sample is different in the various preparations.

More complicated is the explanation of the new line in the spectra. First, one can assume a relaxation of the C_{4v} point symmetry around the Pr^{3+} ion, which could result in further transitions caused by splittings of degenerate lines. If the new line is interpreted in this way, originating from the splitting of the $^3H_4(E')$ level, the same splitting should be observed for other spectral lines, in which this level is involved. The only additional transitions with this level are the $^1D_2(B_2) \rightarrow {}^3H_4(E')$ and $^3P_1(A_2) \rightarrow {}^3H_4(E')$ lines, which do indeed show exactly the same behaviour.

A relaxation of the point symmetry should also result in splittings of other E levels, like for example $^3H_4(E)$ or $^3H_5(E, E', E'')$. However, this is not observed in the spectra, which means either that only the splitting of $^3H_4(E')$ is large enough to become observable or that the new line cannot be explained by a symmetry-induced splitting.

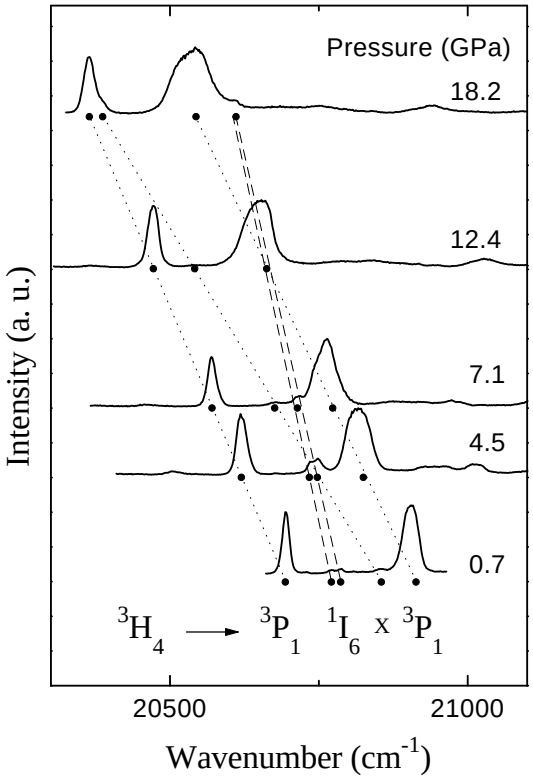

Figure 3. Excitation spectra of Pr^{3+}:LaOCl at various pressures at 60 K. Clearly visible are the different shifts of $^1I_6$ and $^3P_2$ levels.

A different reason for the observation of this new line can be found in the electron–phonon interaction. The interaction between phonons and electronic energy levels can lead to a splitting of the pure electronic states [14]. With changing pressure, the electronic and phonon energies change at different rates. This may result in a resonance for some of these

energies at a specific pressure. In this case, the splitting may be observed only for such an electronic energy level which matches with one specific phonon energy. This model could explain the splitting of $^3H_4(E')$ only. To check this interpretation, Raman scattering experiments are planned to obtain the phonon energies also under pressure.

A typical example for excitation spectra under pressure is shown in figure 3. In this range the transitions $^3H_4 \rightarrow {}^3P_1$ and $^3H_4 \rightarrow {}^1I_6$ can be observed. Clearly visible is the much stronger shift of the $^3P_1$ levels with respect to the $^1I_6$ levels. Up to now the line X at 20 856 cm^{-1} at ambient pressure could not be assigned unambiguously.

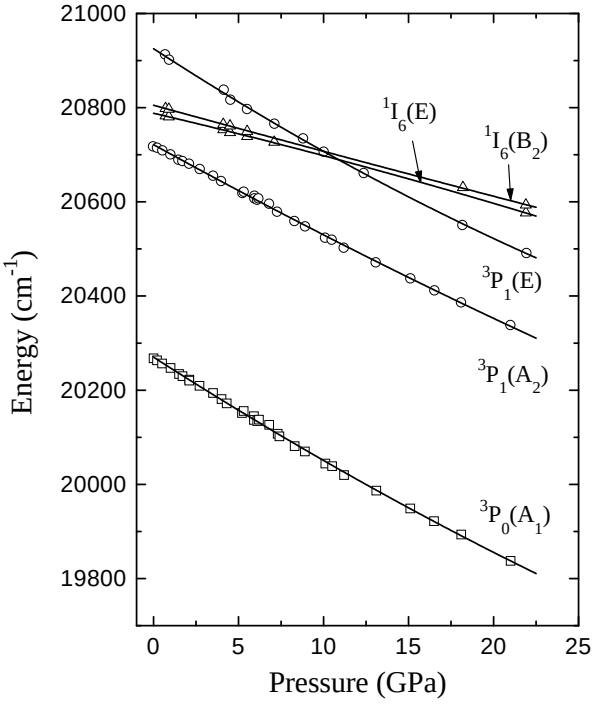

Figure 4. Energies of $^3P_1$, $^1I_6$, and $^3P_0$ under pressure at 20 K.

From the shifts of the spectral lines in figures 2 and 3, it is possible to determine the energy levels $^3P_0(A_1)$, $^3P_1(A_2, E)$, and $^1I_6(E, B_2)$ also under pressure. From their pressure dependence, represented in figure 4, it is then possible to widen the database for the fits of free-ion and crystal-field parameters under pressure.

The variations of the free-ion parameters are shown in figure 5. The solid lines represent the results for the complete data set of the 30 energy levels. As a first result, one can note that the relative decrease of the spin–orbit coupling parameter is smaller than the relative change of the Slater parameter F^2. This is consistent with former results on $Ln^{3+}:LaCl_3$ (Ln = Pr, Nd) [4] and $U^{3+}:LaCl_3$ [5], and supports the former conclusion that a change in the effective nuclear charge alone cannot describe these results. Within this simple screening model, the penetration of the ligand orbitals results in a screening of the effective nuclear charge 'seen' by the f electrons, and the variation of ζ should then be approximately three times larger (for $\Delta\zeta \ll \zeta$) than the variation of F^2, which is not the case in these high-pressure studies.

In such a discussion of free-ion parameters, it is important to know whether the changes

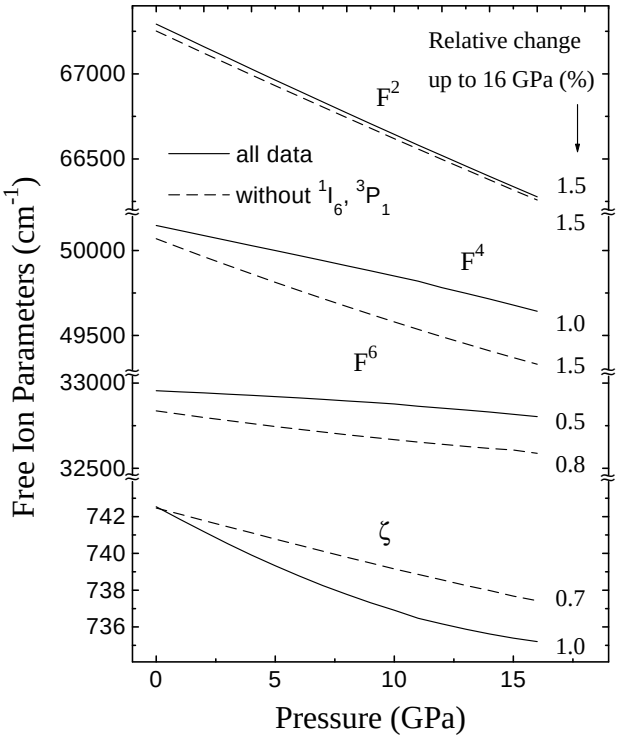

Figure 5. Free-ion parameters F^k ($k = 2, 4, 6$) and ζ for Pr^{3+}:LaOCl under pressure. Solid lines show the results for fits using all energy levels determined under pressure; dashed lines show those for fits without the $^3P_2$ and $^1I_6$ levels.

of the parameters depend critically on the number of levels used in the fits or on the data sets available from experiment. In the former studies no information was available on the $^1I_6$ and $^3P_2$ multiplets. When these energy levels are omitted in the evaluation, one obtains variations of the free-ion parameters as shown by the dashed curves in figure 5.

Obviously, there is a pronounced change in the high-pressure behaviour for most of the free-ion parameters. In particular, the change of the spin–orbit coupling parameter becomes larger, if the $^1I_6$ and $^3P_2$ multiplets are included. This means, that the inclusion of $^1I_6$ and $^3P_2$ in the former studies [4, 5] would also enhance there the variation of ζ with respect to F^2. The present observation of a larger shift of the spin–orbit coupling parameter with respect to the Slater parameters favours to some extent the effective-nuclear-charge model.

Nevertheless, in spite of the increasing change of ζ when including $^1I_6$ and $^3P_2$, the overall change of ζ still remains smaller than the reduction of the Slater parameter F^2. Thus, a simple effective-nuclear-charge model is not sufficient. However, due to this level dependence one must be careful with the use of these parameter shifts in any quantitative analysis.

The changes of the crystal-field parameters are represented in figure 6. Again the solid lines represent the results for the complete data set, and in the case represented by the dashed lines $^1I_6$ and $^3P_2$ levels were omitted. Like for the free-ion parameters, a change of the data set results in different ambient-pressure values as well as in a slightly different high-pressure behaviour for some of the crystal-field parameters.

Particularly interesting is the large change of B_4^6 from 94 cm^{-1} (without $^1I_6$ and $^3P_2$) to

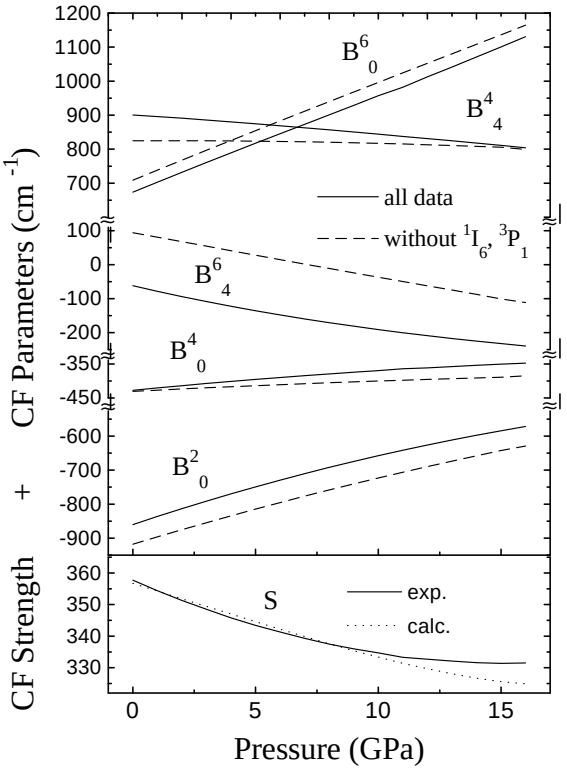

Figure 6. Crystal-field parameters B_q^k ($kq = 20, 40, 44, 60, 64$) for Pr^{3+}:LaOCl under pressure. Solid lines show the results for fits using all energy levels determined under pressure; dashed lines show those for fits without the $^3P_2$ and $^1I_6$ levels. The experimental and theoretical crystal-field strength S are reported at the bottom of the figure as full and dotted lines, respectively.

-62 cm^{-1} (all available data included) at ambient pressure. This large difference shows the sensitivity, especially of B_4^6, on the data set. This means that one has to be careful when one tries to find systematics of crystal-field parameters by comparing different lanthanide ions in the same host. In this case it is practically impossible to rule out large effects on the parameters caused by the use of limited data sets.

Especially for the evaluation of the data with respect to distance dependences, it is important to know whether the high-pressure behaviour depends on the size of the data set. As can be seen in figure 6, the slopes of the parameters are more or less the same whether the complete or the reduced data set is used. Obviously, the slope for the parameter B_4^6 does not depend much on the data set used, although its ambient-pressure value is strongly affected.

From the equation

$$S = \left\{ \frac{1}{3} \sum_k \frac{1}{2k+1} \left[B_{k0}^2 + 2 \sum_{m>0} (\Re B_{km}^2 + \Im B_{km}^2) \right] \right\}^{1/2} \tag{1}$$

it is possible to deduce an overall crystal-field strength [15]. Surprisingly, this crystal-field strength decreases with increasing pressure in the case of Pr^{3+} in LaOCl. Figure 6 shows this crystal-field strength under pressure. This result is consistent with studies on Eu^{3+} in

LaOCl [7], where the crystal-field strength also decreases with increasing pressure.

At first it seems unreasonable to find a decrease in the crystal-field strength when the distances between the lanthanide ion and its ligands decrease under pressure. However, the superposition model [16] offers some explanations through geometrical changes of the lanthanide environment.

First of all, the superposition model reduces the number of crystal-field parameters and introduces the intrinsic parameters $\overline{B}_k(R)$, which depend only on the nature of the ligands and their distances to the lanthanide ion. These intrinsic parameters represent the contribution to the crystal-field strength just from a single ligand. The original crystal-field parameters are calculated from the $\overline{B}_k(R)$ by a summation over the contributions from the different ligands, whereby the intrinsic parameters of a specific ligand have to be multiplied by geometrical factors to transfer all contributions into a common coordinate system:

$$B_q^k = \sum_L \overline{B}_k(R_L) K_{kq}(\Theta_L, \Phi_L) \frac{\alpha_{k0}}{\alpha_{kq}}. \tag{2}$$

The coordination factors K_{kq} as well as values for α_{kq} can be found in the literature [16]. For the distance dependences of the intrinsic parameters, simple power laws are usually assumed:

$$\overline{B}_k(R) = \overline{B}_k(R_0)\left(\frac{R_0}{R}\right)^{t_k} \tag{3}$$

With a convenient value for the reference distance R_0, $\overline{B}_k(R_0)$ and t_k are determined from a fitting of the experimental data.

Table 4. Intrinsic parameters for chlorine and oxygen. The reference distances are: $R_0(\mathrm{Cl}) = 316.74$ pm and $R_0(\mathrm{O}) = 235.3$ pm. The intrinsic parameters originally given by Vishwamittar and Puri for $R_0(\mathrm{O}) = 234.0$ pm, were converted to $R_0(\mathrm{O}) = 235.3$ pm using the exponents determined in the present work. The parameters given by Garcia and Faucher were converted using their own exponents.

	$\overline{B}_2(R_0)$	t_2	$\overline{B}_4(R_0)$	t_4	$\overline{B}_6(R_0)$	t_6
Chlorine						
Present work	196	10.2	315	12.1	253	10.3
Tröster *et al* [4]	—	—	133 (32)	8 (2)	174 (48)	6 (2)
Oxygen						
Present work	887	−4.5	700	4.4	271	3.6
Garcia and Faucher [3]	—	—	821 (117)	5.7	437 (31)	5.9
Vishwamittar and Puri [20]	410 (200)	—	367 (32)	—	423 (48)	—

Thereby, decreasing geometrical factors or intrinsic parameters can be responsible for decreasing crystal-field parameters and therefore a decreasing crystal-field strength. From a preliminary evaluation of high-pressure x-ray and EXAFS data [17], the positions of the five chloride and four oxygen ligands of the host crystal under pressure are known. Taking into account slight local distortions and the crystal-field parameters shown in figure 6, the intrinsic parameters as listed in table 4 are obtained. It has to be noted that the intrinsic parameters depend not only on the variation of the crystal-field parameters, but also on their absolute values. Due to the difficulties in determining these absolute values, an additional offset parameter was introduced in the fits of the intrinsic parameters for any crystal-field

parameter. Therefore, the intrinsic parameters $\overline{B}_k(R_L)$ in table 4 in particular should be regarded as tentative only.

With the intrinsic parameters from table 4, the crystal-field strength is calculated as illustrated in figure 6, where good agreement between experimental and calculated values for S is observed. The comparison of the intrinsic parameters with former results given in table 4 shows reasonable agreement for the absolute values. However, in the present case the exponent t_2(O) is negative. This means, that a specific decrease of the geometrical factors alone cannot explain the decreasing crystal-field strength, but one has to assume a weakening of the interaction between the Pr^{3+} ion and its oxygen ligands for $k = 2$, as the distance decreases.

From *ab initio* calculations it is well known that many different interactions contribute to the intrinsic parameters [18, 19]. These interactions do not enter necessarily with the same signs or the same distance dependences, but result in positive as well as negative contributions. Thus, in general it is possible that an intrinsic parameter has a negative exponent t^k. To check this in the present case, *ab initio* calculations are in progress.

5. Conclusions

Luminescence and excitation measurements on Pr^{3+}:LaOCl determine large parts of the energy level scheme of Pr^{3+}:LaOCl under pressures up to 16 GPa together with the corresponding changes of the free-ion and crystal-field parameters. It is noticed that the free-ion parameters depend strongly on the choice of the energy levels. The multiplets $^1I_6$ and $^3P_2$ have an especially pronounced effect on the variations of the free-ion parameters. Nevertheless, the observed pressure dependences of the free-ion parameters are consistent with former investigations [4, 5], and support the former observation of a restricted validity for the effective-nuclear-charge screening model.

The crystal-field strength decreases by more than 7% from 358 cm^{-1} to 332 cm^{-1} up to 16 GPa. Although quite unexpected, this behaviour can be explained by the superposition model. Within this model, the geometrical factors, multiplied with the intrinsic parameters, lead to an overall decreasing crystal-field strength. However, in this special case the exponent t_2(O) is found to be negative, which shows that not only are the geometrical factors responsible for the decreasing crystal-field strength, but also one observes a weakening of the interaction between the Pr^{3+} ion and its oxygen ligands for $k = 2$ under pressure.

Acknowledgments

This work was supported by the Deutsche Forschungsgemeinschaft (DFG) under grant number HO 486/21 and by the European Community under contract No ERB FMGE*CT95-0017. WBH thanks LENS and its staff for their hospitality during their time of his visit to LENS.

References

[1] Wybourne B G 1965 *Spectroscopic Properties of Rare Earths* (New York: Wiley)
[2] Hüffner S 1978 *Optical Spectra of Transparent Rare Earth Ion Compounds* (New York: Academic)
[3] Garcia D and Faucher M 1995 Crystal field in non-metallic (rare earth) compounds *Handbook on the Physics and Chemistry of Rare Earths* vol 21, ed K A Gschneidner Jr and L Eyring (Amsterdam: North-Holland)
[4] Tröster Th, Gregorian T and Holzapfel W B 1993 *Phys. Rev.* B **48** 2960
[5] Tröster Th and Holzapfel W B 1995 *Phys. Rev.* B **51** 14 892

[6] Shen Y R and Holzapfel W B 1995 *Phys. Rev.* B **51** 15 752
[7] Chi Y, Liu S, Shen W, Wang L and Zou G 1986 *Physica* B **139+140** 555
[8] Jayasankar C K, Reid M F, Tröster Th and Holzapfel W B 1993 *Phys. Rev.* B **48** 5919
[9] Mazurak Z G, van Vliet J P M and Blasse G 1987 *J. Solid State Chem.* **68** 227
[10] Antic-Fidancev E, Lemaitre-Blaise M and Porcher P 1991 *J. Chem. Soc. Faraday Trans.* **87** 3625
[11] Piermarini G J, Block S, Barnet J D and Forman R A 1975 *J. Appl. Phys.* **46** 2774
[12] Noack R A and Holzapfel W B 1979 *High Pressure Science and Technology* vol 1, ed K D Timmerhaus and M S Barber (New York: Plenum) p 748
[13] Le Toullec R, Pinceaux J P and Loubeyre P 1988 *High Pressure Res.* **1** 77
[14] Lupei A and Lupei V 1997 *J. Phys.: Condens. Matter* **9** 2807
[15] Chang N C, Gruber J B, Leavitt R P and Morrison C A 1982 *J. Chem. Phys.* **76** 3877
[16] Newman D J and Ng B 1989 *Rep. Prog. Phys.* **52** 699
[17] Bungenstock C and Holzapfel W B, private communication
[18] Newman D J and Ng B 1986 *J. Phys. C: Solid State Phys.* **19** 389
[19] Shen Y R and Holzapfel W B 1994 *J. Phys.: Condens. Matter* **6** 2367
[20] Vishwamittar and Puri S P 1974 *Phys. Rev.* B **9** 4673